Quantum state transfer on square lattices with topology

Mei-Song Wei, Ming-Jie Liao, Yi-Qing Wang, Zijian Lin, Xingze Qiu, Ce Wang, Jingping Xu,* and Yaping Yang†
MOE Key Laboratory of Advanced Micro-Structured Materials, School of Physics Science and Engineering, Tongji University, Shanghai 200092, China

(Received 8 June 2023; accepted 9 November 2023; published 1 December 2023)

The topological properties of a Heisenberg XY spin model on the square lattice in the form of a two-dimensional Su-Schrieffer-Heeger model is investigated through the quench dynamics. Based on the topological edge states or the higher-order topological corner states of the square lattice, we propose a scheme to transmit quantum states with high quality, including single-excitation state and entangled state, on square lattices. For the transmission of the single-excitation state, when the square lattice is in the topological phase, the maximum fidelity at the corner sites of the lattice is much larger than that of bulk sites. In addition, it has been found that, due to the different symmetries of the spin ladder and the square lattice, the maximally entangled state can be generated between two qubits when a qubit at the edge of the spin ladder is excited initially, while it cannot be generated between two qubits at the corners of the square lattice. However, the maximally entangled state of two qubits at the edge of the spin ladder or the corners of the lattice can both be transmitted to the two qubits at the other side of the lattices with high quality.

DOI: 10.1103/PhysRevA.108.062401

I. INTRODUCTION

An important task in quantum information processing is the transmission of quantum states from one location to another, or the short distance quantum communications. Spin systems have been proved to be one of the most promising candidates for this task in small solid-state devices due to their long decoherence and relaxation time [1–8]. A lot of effort has been devoted to explore efficient schemes to transfer quantum states based on the spin systems [9–14].

On the other hand, the novel topological states, including edge states and higher-order topological corner states, of topological insulators (TIs) [15–20] have attracted lots of attention. These topological states have been theoretically investigated and experimentally found in many other systems including photonic [21–28], acoustic [29–33], mechanical [34–37], and electric circuit [38–42] systems, resulting in the vigorous development of topological physics. Recently, the topological phenomena in spin chains [43] and frustrated skyrmion strings [44] have been explored. It has been found spin chains are equivalent to interacting fermionic chains by Jordan-Wigner transformation [45]. For example, the Heisenberg model with spins interacting with their nearest neighbors by a staggered XXZ and ZZ coupling can be transformed into a fermionic Su-Schrieffer-Heeger (SSH) model [46]. Based on the edge state of the topological spin systems, the quantum state transfer (QST) has also been investigated [47–53].

However, most of the results of quantum states transfer having been reported are based on one-dimensional (1D) topological chain. Entanglement properties in a two-dimensional (2D) triangular [54,55] and square [56] lattices without topology have been investigated, with Ising and XY-type interactions considered. In this work, we investigate the topological properties of Heisenberg spin models with XY-type interactions on a 2D square lattices in the form of a 2D SSH model. Based on the higher-order topological corner states of the 2D SSH model, we investigate the QST on the square lattice. Actually, for the single-excitation subspace considered in this work, the dynamics of the spin model on the lattice has the similar form of a single particle being transferred in the corresponding TI. The difference between these two cases is that, for the transfer of a single particle, the particle is transmitted through the lattice described by the "empty" and "filled" states of the sites, whereas for the QST on the spin model, the excited state (or called the spin-up state) of a qubit is transmitted to other qubits. Also, the QST based on the edge states protected by TIs has been investigated on both 1D [47–50,57–60] and 2D [51–53] lattices. Moreover, the generation and transfer of entangled state measured by Wootters' concurrence [61] are investigated. It has been found, for a finite structure of 2D SSH model in the form of a spin ladder, the entanglement between two qubits can be generated with a high concurrence approach to the maximally entangled state and the initially maximally entangled state can be transmitted through the spin ladder from one side to another with high quality. For a homogeneous square lattice, it has been reported [56] that the entangled state can hardly be transferred on the lattice with a high concurrence when its size increases. In our work, the entangled state can be transmitted between the qubits at corner sites through the square lattice in the form of a 2D SSH model. Our results indicate that the spin model on the lattice in the form of a 2D SSH model with topological properties is a great candidate for quantum entanglement transfer in small solid-state devices.

*xx_jj_pp@tongji.edu.cn
†yang_yaping@tongji.edu.cn

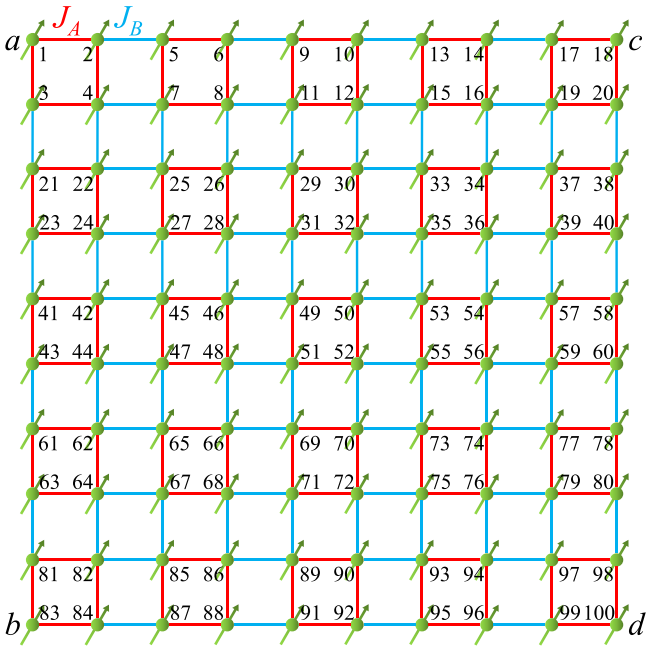

FIG. 1. The XY spin model on a square lattice with the size $L = M = 5$. The parameter $J_A(J_B)$ is the strength of the intracell (intercell) coupling.

The remainder of this paper is organized as follows. In Sec. II, we describe the topological properties of the spin model on the square lattice and explore the phase transition through the quench dynamics. In Sec. III, we explore the QST on a spin ladder in the topological phase. In Sec. IV, the QST on a square lattice in the form of a 2D SSH model is also discussed. Conclusions are presented in Sec. V.

II. SPIN MODEL ON THE SQUARE LATTICE

In this section, we consider a transverse field XY spin model on a square lattice shown in Fig. 1. The size of the square lattice is $L \times M$, indicating that the square lattice has L unit cells along one direction and has M unit cells along the other direction and the total number of the sites is $N = 4(L \times M)$. The site numbers are marked as Fig. 1 shows with a, b, c, and d representing the four spins on the corner sites. The Hamiltonian of the system is given by

$$H = \sum_{\langle ij \rangle} J_{ij}\left(s_i^x s_j^x + s_i^y s_j^y\right) + \mu \sum_i s_i^z. \tag{1}$$

The parameter J_{ij} is the coupling strength between nearest-neighbor spins, μ is the strength of the transverse field, and $\vec{s}_i = (s_i^x, s_i^y, s_i^z)$ is the spin-1/2 operators of the ith spin. The spin model can be experimentally realized by some platforms, including ultracold atoms in optical lattices [62], trapped ions [63], and quantum dots [64]. The couplings J_i can be created in these systems. Taking the ultracold atoms in optical lattices as an example [65], the couplings can be tuned by additional laser beams or the spatial light modulator technology, which, in principle, can create arbitrary potentials and couplings for ultracold atoms.

With the relations

$$\vec{s} = \frac{\hbar}{2}\vec{\sigma},\ \sigma_i^{\pm} = \frac{1}{2}\left(\sigma_i^x \pm i\sigma_i^y\right), \tag{2}$$

the Hamiltonian can be written in terms of Pauli operators as (taking $\hbar = 1$)

$$H = \sum_{\langle ij \rangle} \frac{J_{ij}}{2}(\sigma_i^+\sigma_j^- + \sigma_i^-\sigma_j^+) + \mu \sum_i \left(\sigma_i^+\sigma_i^- - \frac{1}{2}\right). \tag{3}$$

In the following, considering the strengths of the interactions as

$$J_A = 2\kappa(1+\lambda),\ J_B = 2\kappa(1-\lambda),\ (0 \leqslant \lambda \leqslant 1), \tag{4}$$

we have

$$H = \sum_{\langle ij \rangle} \kappa_{ij}(\sigma_i^+\sigma_j^- + \sigma_i^-\sigma_j^+) + \mu \sum_i \sigma_i^+\sigma_i^-, \tag{5}$$

where κ_{ij} take two kinds of value

$$\kappa_A = \kappa(1+\lambda),\ \kappa_B = \kappa(1-\lambda). \tag{6}$$

We consider the specific form for the couplings J_A and J_B here to obtain a lattice in the form of a 2D SSH model, which consists of four sites per unit cell with dimerized nearest-neighbor hoppings. Then, J_A is the intracell hopping, and J_B is the intercell hopping. The constant $-\mu/2$ is dropped here because it has no effect on the evolution of the system. This Hamiltonian is in the form of a 2D SSH model with the first term being the hopping part and the second term being the on-site potential.

We consider a normalized single-excitation state for the spin model on the square lattice

$$|\psi\rangle = \sum_{n=1}^{N} \psi_n |n\rangle, \tag{7}$$

where

$$|n\rangle = |0\rangle_1 \otimes |0\rangle_2 \otimes \cdots |1\rangle_n \otimes \cdots \tag{8}$$

represents that the nth spin is excited while others are at ground state. In the single-excitation subspace, the Hamiltonian H can be written as a $N \times N$ matrix $\{H_{mn}\}_{N\times N}$:

$$H = \sum_{mn} H_{mn}|m\rangle\langle n|. \tag{9}$$

For the single-excitation subspace considered here, the matrix $\{H_{mn}\}$ in Eq. (9) is equivalent to that of a standard tight-binding Hamiltonian for a single particle moving on a square lattice.

It is known the 2D SSH model has chiral symmetry as well as C_{4v} symmetry and the band structure in the lattice is in a topological phase for $-1 < \lambda < 0$ and in a trivial phase for $0 < \lambda < 1$. In the following, we take a square lattice with the size $L = M = 5$. The energy eigenvalues E_j $(j = 1, 2, \ldots, N)$ of such a finite structure, in units of κ, are shown in Fig. 2(a). The second-order topological corner states corresponding to the zero-energy modes (red lines) as well as the edge modes (cyan lines) emerge for $-1 < \lambda < 0$. Figure 2(b) shows the energy eigenvalues of the system with $\lambda = -0.5$.

The density of several eigenstates of the system in the topological phase with $\lambda = -0.5$ are shown in Fig. 3. A bulk

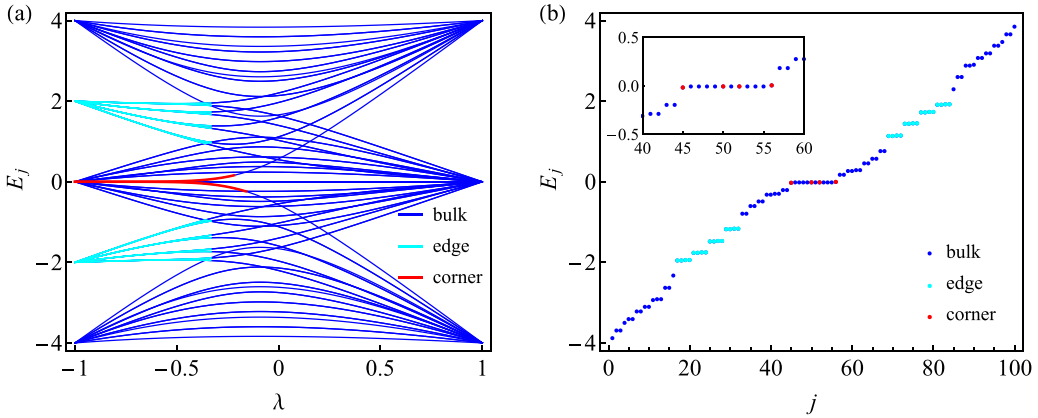

FIG. 2. (a) The energy spectrum of a finite lattice with the size $L = M = 5$. (b) The energy eigenvalues (in units of κ) of the spin model on the lattice with $\lambda = -0.5$.

state is shown in Fig. 3(a), where the probability amplitude of the state is mainly distributed on the bulk sites. One of the edge state is shown in Fig. 3(b), and the probability amplitude of the state is mainly distributed on the edge sites. Figure 3(c) is one of the corner states, and the probability amplitude of the state becomes small except for the four corners. These corner states are bound states in the continuum due to these zero-energy modes existing in the continuous band structure. The edge states and corner states vanish when the system is in the trivial phase.

The system evolves under the equation

$$i\frac{d}{dt}\psi_n(t) = \sum_{m=1}^{N} H_{nm}\psi_m(t) + \mu\psi_n(t), \tag{10}$$

then the time-dependent single-excitation state is

$$|\psi(t)\rangle = \sum_{n=1}^{N} \psi_n(t)|n\rangle. \tag{11}$$

The time evolution equation (10) can be solved by

$$|\psi(t)\rangle = \sum_{i=1}^{N} C_i e^{-iE_i t}|\phi_i\rangle, \tag{12}$$

where E_i and $|\phi_i\rangle$ are the ith eigenvalue and the ith eigenstate of the Hamiltonian H and $C_i = \langle\phi_i|\psi(0)\rangle$.

The topological property of a topological system can be expressed by the quench dynamics [66,67], where a pulse is given to one site and its time evolution described by Eq. (10) is explored. During the process of the quench dynamics, the initial state is prepared in an eigenstate of a Hamiltonian H_1, and then this state evolves under another Hamiltonian H_2, which is a new Hamiltonian carried out by suddenly changing some parameters of H_1. Here, we prepare the initial state as $|\psi(0)\rangle = |1\rangle$, which is an eigenstate of the Hamiltonian H in Eq. (9) with $\lambda = -1$. Then, the system evolves under the Hamiltonian H by suddenly changing the parameter λ. With the initial condition $\psi_1(0) = 1$, i.e., the spin on the first site of a square lattice of a finite size $L = M = 5$ is on the excited state at the beginning, we plot the amplitude $|\psi_1|$ varies with λ at the time $\kappa t = 10$ in Fig. 4. It is shown that the amplitude $|\psi_1|$ is a finite value when the system is in the topological phase, while it is almost zero in the trivial phase. The finite value near $\lambda = 1$ corresponding to the tetramer phase, where the system is decomposed into a set of tetramers with the tetramer limit $\lambda = 1$, and the energy is transmitted only in the first cell. When it is expanded with the eigenstates of the Hamiltonian H, the components of the initial state $|\psi(0)\rangle = |1\rangle$ considered here are mainly the corner states in the topological phase. The evolution speed is mainly dependent on the narrow gap between the eigenvalues

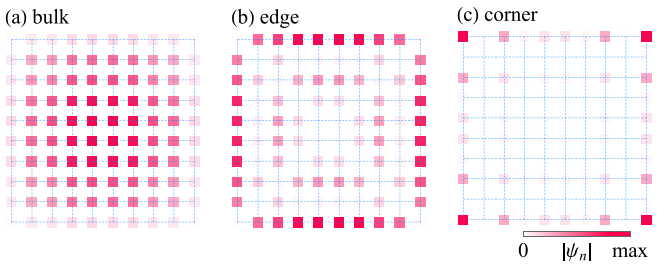

FIG. 3. Density of (a) a bulk state, (b) an edge state, and (c) a corner state. The lattice is in the topological phase with $\lambda = -0.5$.

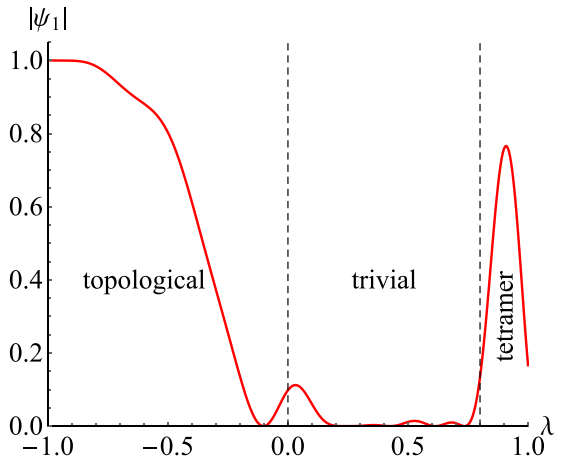

FIG. 4. The probability amplitude of the first spin staying at the excited state when the system evolves to the state at the time $\kappa t = 10$.

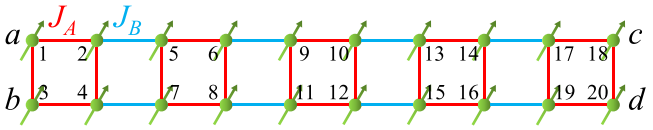

FIG. 5. A spin ladder with the size $L \times M = 5 \times 1$.

corresponding to the corner states, so the presence of the higher-order corner states makes the particle tend to spend time at this corner site. Moreover, a much stronger indicator of a nontrivial topology is the topological invariant. For the 2D SSH model, the topological invariant Zak phase has been calculated in some works [68,69], where the Zak phases along the x and y directions are $P_x = P_y = 1/2$ for the topological phase and $P_x = P_y = 0$ for the trivial phase.

III. QUANTUM STATE TRANSFER ON A SPIN LADDER

We first discuss the dynamics of qubits on a square lattice with the size 5×1 in the form of a so-called spin ladder shown in Fig. 5. This spin ladder can be regarded as parallel spin-chain channels with the couplings between the spins on the two parallel spin chains and the entanglement transfer on the channels with homogeneous spin chains has been investigated. The two coupled spin chains discussed here are in the form of the SSH model.

Figure 6 is the time evolution of the spin ladder with the initial state $|\psi(0)\rangle = |1\rangle_1 \otimes \prod_{n\neq 1} |0\rangle_n$, meaning that only the first spin (qubit a) is excited initially. Figures 6(a1) to 6(a5) present the evolution of the system in the topological phase ($\lambda = -0.5$). The corner states of a square lattice will degenerate to the edge states like that of the 1D SSH model when the lattice is of such a size. Due to the existences of the edge states, the exchange of energy is mainly concentrated on the edge sites, and less energy will flow into the bulk sites. Figures 6(b1) to 6(b5) describe the system evolving in the

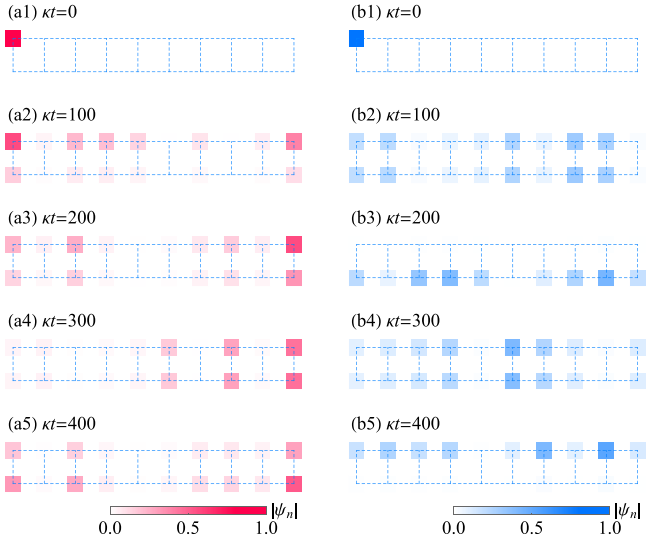

FIG. 6. Time evolution of the spin ladder with the first spin being excited initially. The parameters are set as (a1)–(a5) $\lambda = -0.5$ (topological) and (b1)–(b5) $\lambda = 0.5$ (trivial).

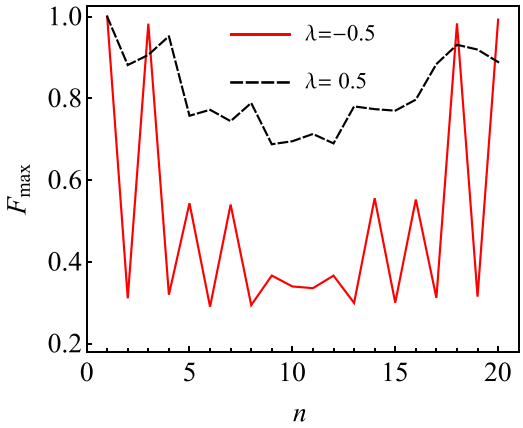

FIG. 7. The maximum fidelity $F_{\max}$ on each site of the spin ladder in a time interval $0 \leqslant \kappa t \leqslant 1000$, with the initial state $|\psi(0)\rangle = |1\rangle_1 \otimes \prod_{n\neq 1} |0\rangle_n$. The parameters are set as $\lambda = -0.5$ for the topological phase and $\lambda = 0.5$ for the trivial phase.

topological phase ($\lambda = 0.5$). In this case, the energy flows into the bulk sites irregularly due to the absence of the edge state.

The time evolution of the system shown in Fig. 6 can be treated as a problem of QST with a single excitation on the first spin qubit. To describe the quality of the QST on the lattice, we employ the wildly used fidelity defined as

$$F(t) = \sqrt{\langle\psi_1(0)|\rho_i(t)|\psi_1(0)\rangle}, \tag{13}$$

where $|\psi_1(0)\rangle$ is the initial state of the first spin (sender) and $\rho_i(t)$ is the reduced density matrix of the ith spin (receiver) at time t. The fidelity $F = 1$ indicates a perfect QST from one site to another. In this way, we discuss the quality of the QST from the first qubit to other qubits on the lattice through the maximum fidelity $F_{\max}$ at each site. In Fig. 7, we plot the maximum fidelity $F_{\max}$ at each site of the spin ladder, where the maximum fidelity $F_{\max}$ is obtained in a time interval $0 \leqslant \kappa t \leqslant 1000$. Due to the existence of the edge states in the topological phase with $\lambda = -0.5$, the values of $F_{\max}$ at the edge sites are much larger than that at the bulk sites. While in the trivial phase with $\lambda = 0.5$, $F_{\max}$ has an increase on each bulk site, but it becomes lower at the edge sites.

Next, we discuss the dynamics of the entanglement of a two-qubit system. The density matrix of the whole system is $\rho(t) = |\psi(t)\rangle\langle\psi(t)|$. We focus on the evolution of the entanglement of two qubits, for example, spins a and b (or c and d), and the others spins are treated as the environment E. These spins are marked in Fig. 5. So we derive the reduced density matrix $\rho_S(t)$ of the two qubits through a partial trace operation to $\rho(t)$,

$$\rho_S(t) = \mathrm{Tr}_E[\rho(t)], \tag{14}$$

which trace out the degrees of freedom of all the other spins. In the basis $\{|00\rangle, |01\rangle, |10\rangle, |11\rangle\}$, the reduced density matrix $\rho_S(t)$ is a 4×4 matrix. For two spin-1/2 qubits, the entanglement can be measured by Wootters' concurrence defined as [61]

$$C(\rho_S) = \max\{\sqrt{\lambda_1} - \sqrt{\lambda_2} - \sqrt{\lambda_3} - \sqrt{\lambda_4}, 0\}, \tag{15}$$

where $\lambda_1 \geqslant \lambda_2 \geqslant \lambda_3 \geqslant \lambda_4$ are the eigenvalues of the matrix $\rho_S(\sigma^y \otimes \sigma^y)\rho_S^*(\sigma^y \otimes \sigma^y)$. The two qubits are maximally

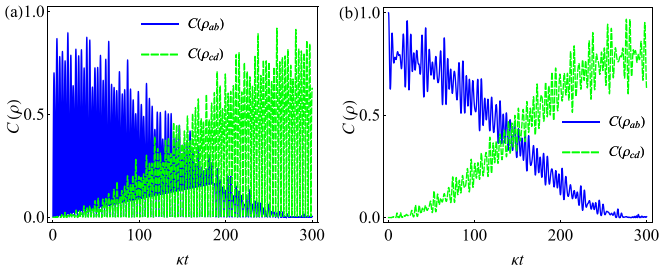

FIG. 8. (a) Evolution of the entanglement between qubits a and b (c and d) on a spin ladder. (b) Entanglement transfer from qubits a and b to qubits c and d on a spin ladder, described by the concurrence C as a function of κt. The initial states are (a) $|\psi(0)\rangle = |1\rangle_1 \otimes \prod_{n\neq 1} |0\rangle_n$ and (b) $|\psi(0)\rangle = \frac{1}{\sqrt{2}}(|1\rangle_a|0\rangle_b + |0\rangle_a|1\rangle_b)$ and the parameter is set as $\lambda = -0.5$.

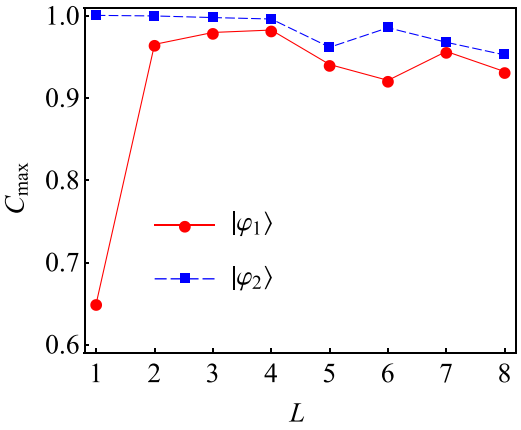

FIG. 9. The maximum concurrence $C_{\max}$ of the qubits c and d on the spin ladder for different sizes L ($M = 1$) in a time interval $0 \leqslant \kappa t \leqslant 10\,000$, with the initial state $|\varphi_1\rangle = |1\rangle_1 \otimes \prod_{n\neq 1} |0\rangle_n$ and $|\varphi_2\rangle = \frac{1}{\sqrt{2}}(|1\rangle_a|0\rangle_b + |0\rangle_a|1\rangle_b)$. The parameter is set as $\lambda = -0.5$.

entangled for concurrence $C = 1$ and there exists no entanglement between the two qubits when concurrence $C = 0$.

With the topological edge states and higher-order corner states, we would like to realize the entanglement transfer from one side (or corner) to another side in the topological phase. In Fig. 8(a), we plot the concurrence C as a function of κt to express the evolution of the entanglement between two qubits with the initial state $|\psi(0)\rangle = |1\rangle_1 \otimes \prod_{n\neq 1} |0\rangle_n$. At the beginning, only the qubit a is excited. With the system evolving, the qubit a will interact with its closest site, qubit b, resulting in the generation of the entanglement between qubits a and b. Then, the energy is transmitted as Fig. 6 shows, and finally, the entanglement between c and d is generated. Since the initial state of the system is $|\psi(0)\rangle = |1\rangle$, and there is no entanglement between qubits at the beginning. However, when the system is in the topological phase, the entanglement between two qubits can be generated through the interaction between spins with less energy flowing into the environment.

In Fig. 8(b), the concurrence C as a function of κt with the initial state $|\psi(0)\rangle = \frac{1}{\sqrt{2}}(|1\rangle_a|0\rangle_b + |0\rangle_a|1\rangle_b)$ is plotted. In this case, qubits a and b are prepared as a maximally entangled state initially with concurrence $C_{ab} = 1$, and we are concerned with the transfer of the entanglement from qubits a and b to qubits c and d. As is shown in Fig. 8(b), with the concurrence of qubits a and b decaying, the concurrence of qubits c and d rises gradually. Due to the tiny values of the probability amplitudes of bulk sites for the topological edge or corner states, the energy of qubits a and b may not be transmitted to c and d completely. For this reason, the state obtained at the edge with qubits c and d will be a state approaching to a maximally entangled one. So the entanglement can be transmitted through the topological spin ladder with high quality. One may hope to obtain a the maximally entangled state after the transmission of the state, so the stop of the transmission should be considered when needed. In addition, one way to control the start and stop of the transmission is switching on and off the weak couplings, which has been applied in many works [48,49,58].

In Fig. 9, we explore the influence of the size of the spin ladder on the maximum value of the entanglement between qubits c and d during the evolution of the system. For a topological structure, the size of the lattice has a huge impact on the QST time, so we evaluate the maximum concurrence $C_{\max}$ in a large time interval $0 \leqslant \kappa t \leqslant 10\,000$. On the spin ladder, when the initial state is $|\varphi_1\rangle = |1\rangle_1 \otimes \prod_{n\neq 1} |0\rangle_n$, $C_{\max}$ has an evident improvement with the size L increasing from 1 to 2. When the size is $L = 1$, the lattice contains only one cell with four spins, and the transfer time of the energy from a to d is longer than that of from a to c, resulting in a small $C_{\max}$. For the initial state $|\varphi_2\rangle = \frac{1}{\sqrt{2}}(|1\rangle_a|0\rangle_b + |0\rangle_a|1\rangle_b)$, $C_{\max}$ has a slight decrease with the size L increasing, which is caused by the increase of the amount of environmental spins.

IV. QUANTUM STATE TRANSFER ON A SQUARE LATTICE

In this section, we analyze the dynamics of spin qubits on a square lattice with size 5×5, in the form of a 2D SSH model, shown in Fig. 1.

In Fig. 10, we initially prepare the first spin at the excited state and plot the time evolution of the square lattice. Figures 10(a1) to 10(a5) describe the evolution of the lattice in the topological phase, and in this case, the system will evolve mainly in the form of the superposition of the corner states according to Eq. (12). The energy of the first spin is transmitted through the lattice in the form of the propagation of a weak wave and is mainly distributed on the corner sites and the sites near the four corners. The transmission of the energy is in a symmetrical form due to the symmetry of the square lattice with the axis ad, with spins a, b, c, and d marked in Fig. 1. Figures 10(b1) to 10(b5) show the evolution of the lattice in the trivial phase. The symmetry of the transmission of the energy also exists in the trivial phase. However, due to the absence of the topological corner state, the distribution of the density of the state is mainly on the bulk sites.

The maximum fidelity $F_{\max}$ at each site of the square lattice is shown in Fig. 11, with maximum fidelity $F_{\max}$ obtained in a time interval $0 \leqslant \kappa t \leqslant 1000$. The QST on a square lattice with $\lambda = 0$ ($J_A = J_B$) was studied in Ref. [56]. It was reported that the maximum fidelity $F_{\max}$ on the square lattice is in the form of the central symmetry. As is shown in Fig. 11(a), in the topological phase, when qubit a is stimulated at the beginning, the maximum fidelity $F_{\max}$ of qubit d has the highest value,

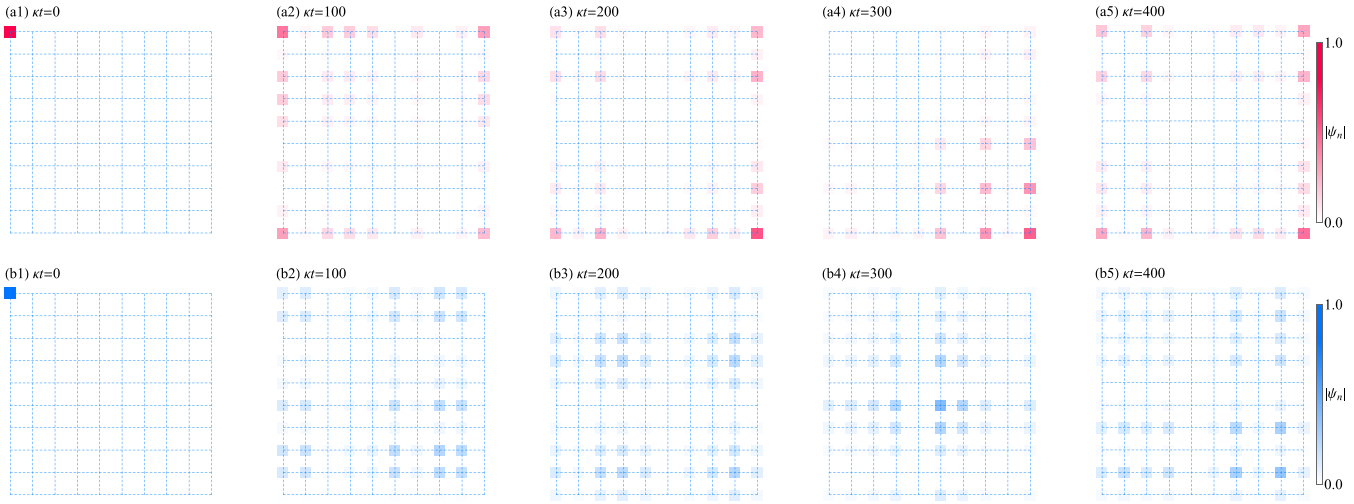

FIG. 10. Time evolution of the XY model on the square lattice with the first spin being excited initially. The parameters are set as (a1)–(a5) $\lambda = -0.5$ (topological) and (b1)–(b5) $\lambda = 0.5$ (trivial).

while $F_{\max}$ at other sites are much lower. In Fig. 11(b), when the system is in the trivial phase, $F_{\max}$ of other qubits is increased, also in a form of the central symmetry. Although the maximum fidelity $F_{\max}$ of on the trivial lattice has an overall improvement, the QST on the lattice is disordered as shown Figs. 10(b1) to 10(b5).

The time evolution of the entanglement between qubits measured by the concurrence C is shown in Fig. 12(a), where the initial state of the system is $|\psi(0)\rangle = |1\rangle_1 \otimes \prod_{n\neq 1} |0\rangle_n$. Like the case of the spin ladder, although there is no entanglement between qubits at the beginning, the entanglement between qubits a and b can also be generated through the environment spin qubits on the lattice, and then, the entanglement between qubits a and b is transmitted to qubits c and d through the lattice. Different from that in the spin ladder, the entanglement will not reach to the maximum even the time is long enough. It can be explained by the evolution in Figs. 10(a1) to 10(a5), the energy of spin a propagates through a longer path to qubit d than it propagates to qubit c. So the energy is almost impossible to mainly and equally distribute on qubits c and d and the entanglement can not reach to the maximum for this reason.

The concurrence C as a function of κt with qubits a and b initially prepared in a maximally entangled state $|\psi(0)\rangle = \frac{1}{\sqrt{2}}(|1\rangle_a|0\rangle_b + |0\rangle_a|1\rangle_b)$ is also plotted in Fig. 12(b). Similar to the time evolution of the spin ladder shown in Fig. 8, the entanglement between qubits c and d is gradually generated and reaches to the maximum (about 0.95) with the decay of the entanglement between qubits a and b. The oscillations on the curve, which also exist in Fig. 8(b), represent the interactions between the environmental spins, and the larger amplitudes of oscillations in Fig. 12(b) indicate more environmental spins in the square lattice than in the spin ladder. When the energy is distributed to qubits a and b equally at the beginning, the transmission of the energy from qubits a and b to qubits c and d is symmetrical along the horizontal direction so the maximally entangled state can be transmitted through the lattice with a high maximum concurrence, although not perfectly. This is different from the results of the case of the product state shown in Fig. 12(a).

The influence of the size of the square lattice on the maximum value of the entanglement between qubits c and d during the evolution of the system is shown in Fig. 13.

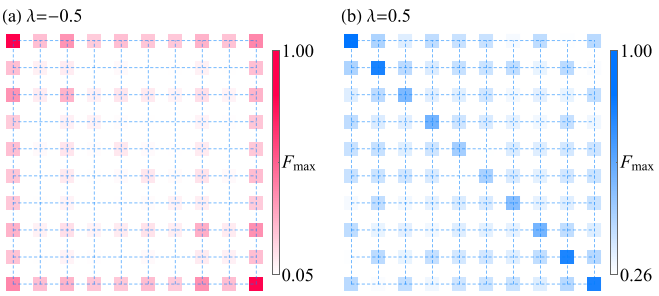

FIG. 11. The maximum fidelity $F_{\max}$ on each site of the lattice in a time interval $0 \leqslant \kappa t \leqslant 1000$, with the initial state $|\psi(0)\rangle = |1\rangle_1 \otimes \prod_{n\neq 1} |0\rangle_n$. The parameters are set as (a) $\lambda = -0.5$ and (b) $\lambda = 0.5$.

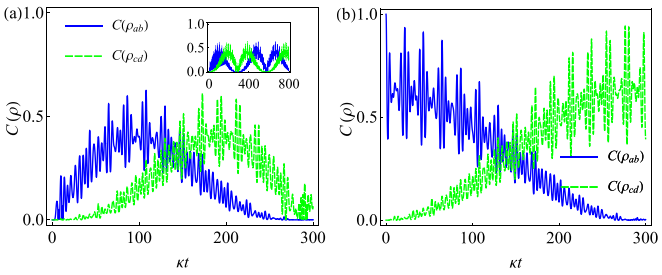

FIG. 12. (a) Evolution of the entanglement between qubits a and b (c and d) and (b) entanglement transfer from qubits a and b to qubits c and d on a square lattice, described by the concurrence C as a function of κt. The initial states are (a) $|\psi(0)\rangle = |1\rangle_1 \otimes \prod_{n\neq 1} |0\rangle_n$ and (b) $|\psi(0)\rangle = \frac{1}{\sqrt{2}}(|1\rangle_a|0\rangle_b + |0\rangle_a|1\rangle_b)$, and the parameter is set as $\lambda = -0.5$.

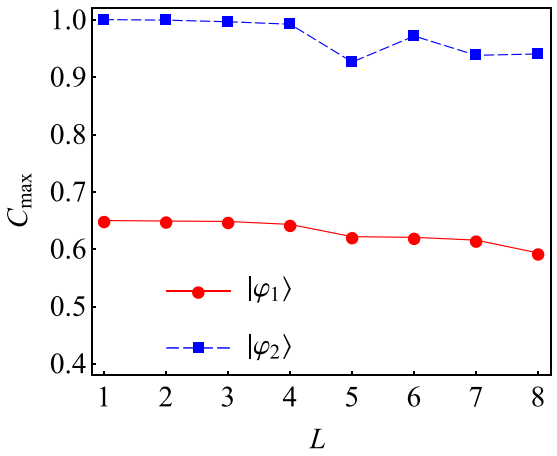

FIG. 13. The maximum concurrence $C_{\max}$ of the qubits c and d on the square lattice for different sizes L ($M = L$) in a time interval $0 \leqslant \kappa t \leqslant 10\,000$, with the initial state $|\varphi_1\rangle = |1\rangle_1 \otimes \prod_{n\neq 1} |0\rangle_n$ and $|\varphi_2\rangle = \frac{1}{\sqrt{2}}(|1\rangle_a|0\rangle_b + |0\rangle_a|1\rangle_b)$. The parameter is set as $\lambda = -0.5$.

For the initial state $|\varphi_1\rangle = |1\rangle_1 \otimes \prod_{n\neq 1} |0\rangle_n$, $C_{\max}$ remains a small value. Because, on the square lattice, the difference between the paths of transmission from a to c and from a to c keeps huge with the increase of size L. For the initial state $|\varphi_2\rangle = \frac{1}{\sqrt{2}}(|1\rangle_a|0\rangle_b + |0\rangle_a|1\rangle_b)$, $C_{\max}$ also has a slight decrease with the size L increasing, which is similar with that shows in Fig. 9.

V. CONCLUSION

In conclusion, through the quench dynamics, we investigated the topological properties of a Heisenberg XY spin model on the square lattice, in the form of a 2D SSH model. Based on the topological edge states of the spin ladder and the higher-order topological corner states of the square lattice, we explored the time evolution and transfer of quantum states including single-excitation state and entangled state on the lattices. For the transmission of a single-excitation state, the first spin at the corner site of the spin ladder and square lattice is stimulated initially. It has been found that, at the edge sites of the spin ladder or the corner sites the square lattice, the maximum fidelity is much larger than that at the bulk sites when the systems are in the topological phase. Specifically, on the square lattice, the distribution of the maximum fidelity is in the form of the central symmetry. In addition, the state approaching to a maximally entangled state can be generated between two qubits when a qubit on the edge of the spin ladder is excited initially, and the maximally entangled state between two qubits at one edge of the spin ladder can be transmitted to the two qubits at the other edge with high quality. While for the square lattice, the maximally entangled state cannot be generated when only one qubit at a corner of the lattice is excited initially due to the different paths of the propagation of the energy. However, due to the symmetry of the square lattice, when two qubits at the corners of the lattice is maximally entangled at the beginning, the maximally entangled state can also be transmitted to the two qubits at the other two corners with high quality. Our results provide an effective scheme to transmit quantum entanglement in small solid-state devices.

ACKNOWLEDGMENTS

This work is supported by the National Natural Science Foundation of China (Grants No. 12174288, No. 12204352, and No. 12274326) and the National Key R & D Program of China (Grant No. 2021YFA1400602).

[1] D. Loss and D. P. DiVincenzo, Quantum computation with quantum dots, Phys. Rev. A **57**, 120 (1998).
[2] B. E. Kane, A silicon-based nuclear spin quantum computer, Nature (London) **393**, 133 (1998).
[3] G. Burkard, D. Loss, and D. P. DiVincenzo, Coupled quantum dots as quantum gates, Phys. Rev. B **59**, 2070 (1999).
[4] R. Raussendorf and H. J. Briegel, A one-way quantum computer, Phys. Rev. Lett. **86**, 5188 (2001).
[5] T. D. Ladd, J. R. Goldman, F. Yamaguchi, Y. Yamamoto, E. Abe, and K. M. Itoh, All-silicon quantum computer, Phys. Rev. Lett. **89**, 017901 (2002).
[6] A. J. Skinner, M. E. Davenport, and B. E. Kane, Hydrogenic spin quantum computing in silicon: A digital approach, Phys. Rev. Lett. **90**, 087901 (2003).
[7] S. Bose, Quantum communication through an unmodulated spin chain, Phys. Rev. Lett. **91**, 207901 (2003).
[8] R. de Sousa, J. D. Delgado, and S. Das Sarma, Silicon quantum computation based on magnetic dipolar coupling, Phys. Rev. A **70**, 052304 (2004).
[9] N. Khaneja and S. J. Glaser, Efficient transfer of coherence through Ising spin chains, Phys. Rev. A **66**, 060301(R) (2002).
[10] F. Verstraete, M. A. Martín-Delgado, and J. I. Cirac, Diverging entanglement length in gapped quantum spin systems, Phys. Rev. Lett. **92**, 087201 (2004).
[11] M. Christandl, N. Datta, A. Ekert, and A. J. Landahl, Perfect state transfer in quantum spin networks, Phys. Rev. Lett. **92**, 187902 (2004).
[12] D. Burgarth and S. Bose, Conclusive and arbitrarily perfect quantum-state transfer using parallel spin-chain channels, Phys. Rev. A **71**, 052315 (2005).
[13] J. Fitzsimons and J. Twamley, Globally controlled quantum wires for perfect qubit transport, mirroring, and computing, Phys. Rev. Lett. **97**, 090502 (2006).
[14] V. Giovannetti and D. Burgarth, Improved transfer of quantum information using a local memory, Phys. Rev. Lett. **96**, 030501 (2006).
[15] M. Z. Hasan and C. L. Kane, Colloquium: Topological insulators, Rev. Mod. Phys. **82**, 3045 (2010).
[16] X.-L. Qi and S.-C. Zhang, Topological insulators and superconductors, Rev. Mod. Phys. **83**, 1057 (2011).
[17] J. Langbehn, Y. Peng, L. Trifunovic, F. von Oppen, and P. W. Brouwer, Reflection-symmetric second-order topological insulators and superconductors, Phys. Rev. Lett. **119**, 246401 (2017).

[18] F. Schindler, A. M. Cook, M. G. Vergniory, Z. Wang, S. S. P. Parkin, B. A. Bernevig, and T. Neupert, Higher-order topological insulators, Sci. Adv. **4**, eaat0346 (2018).

[19] M. Ezawa, Higher-order topological insulators and semimetals on the breathing Kagome and pyrochlore lattices, Phys. Rev. Lett. **120**, 026801 (2018).

[20] M. Ezawa, Topological switch between second-srder topological insulators and topological crystalline insulators, Phys. Rev. Lett. **121**, 116801 (2018).

[21] A. B. Khanikaev, S. H. Mousavi, W.-K. Tse, M. Kargarian, A. H. MacDonald, and G. Shvets, Photonic topological insulators, Nat. Mater. **12**, 233 (2013).

[22] M. Hafezi, E. Demler, M. Lukin, and J. Taylor, Robust optical delay lines with topological protection, Nat. Phys. **7**, 907 (2011).

[23] M. Hafezi, S. Mittal, J. Fan, A. Migdall, and J. Taylor, Imaging topological edge states in silicon photonics, Nat. Photonics **7**, 1001 (2013).

[24] L. Lu, J. D. Joannopoulos, and M. Soljacic, Topological photonics, Nat. Photonics **8**, 821 (2014).

[25] A. B. Khanikaev and G. Shvets, Two-dimensional topological photonics, Nat. Photonics **11**, 763 (2017).

[26] B. Bahari, A. Ndao, F. Vallini, A. E. Amili, Y. Fainman, and B. Kanté, Nonreciprocal lasing in topological cavities of arbitrary geometries, Science **358**, 636 (2017).

[27] T. Ozawa, H. M. Price, A. Amo, N. Goldman, M. Hafezi, L. Lu, M. C. Rechtsman, D. Schuster, J. Simon, O. Zilberberg, and I. Carusotto, Topological photonics, Rev. Mod. Phys. **91**, 015006 (2019).

[28] M. Li, D. Zhirihin, D. Filonov, X. Ni, A. Slobozhanyuk, A. Alù, and A. B. Khanikaev, Higher-order topological states in photonic Kagome crystals with long-range interactions, Nat. Photonics **14**, 89 (2020).

[29] Z. Yang, F. Gao, X. Shi, X. Lin, Z. Gao, Y. Chong, and B. Zhang, Topological acoustics, Phys. Rev. Lett. **114**, 114301 (2015).

[30] P. Wang, L. Lu, and K. Bertoldi, Topological phononic crystals with one-way elastic edge waves, Phys. Rev. Lett. **115**, 104302 (2015).

[31] C. He, X. Ni, H. Ge, X.-C. Sun, Y.-B. Chen, M.-H. Lu, X.-P. Liu, L. Feng, and Y.-F. Chen, Acoustic topological insulator and robust one-way sound transport, Nat. Phys. **12**, 1124 (2016).

[32] H. Xue, Y. Yang, F. Gao, Y. Chong, and B. Zhang, Acoustic higher-order topological insulator on a kagome lattice, Nat. Mater. **18**, 108 (2019).

[33] X. Ni, M. Weiner, A. Alu, and A. B. Khanikaev, Observation of higher-order topological acoustic states protected by generalized chiral symmetry, Nat. Mater. **18**, 113 (2019).

[34] B. G.-G. Chen, N. Upadhyaya, and V. Vitelli, Nonlinear conduction via solitons in a topological mechanical insulator, Proc. Natl. Acad. Sci. USA **111**, 13004 (2014).

[35] L. M. Nash, D. Kleckner, A. Read, V. Vitelli, A. M. Turner, and W. T. M. Irvine, Topological mechanics of gyroscopic metamaterials, Proc. Natl. Acad. Sci. USA **112**, 14495 (2015).

[36] J. Paulose, A. S. Meeussen, and V. Vitelli, Selective buckling via states of self-stress in topological metamaterials, Proc. Natl. Acad. Sci. USA **112**, 7639 (2015).

[37] R. Süsstrunk and S. D. Huber, Observation of phononic helical edge states in a mechanical topological insulator, Science **349**, 47 (2015).

[38] C. H. Lee, S. Imhof, C. Berger, F. Bayer, J. Brehm, L. W. Molenkamp, T. Kiessling, and R. Thomale, Topolectrical circuits, Commun. Phys. **1**, 39 (2018).

[39] S. Imhof, C. Berger, F. Bayer, J. Brehm, L. Molenkamp, T. Kiessling, F. Schindler, C. H. Lee, M. Greiter, T. Neupert, and R. Thomale, Topolectrical-circuit realization of topological corner modes, Nat. Phys. **14**, 925 (2018).

[40] M. Ezawa, Higher-order topological electric circuits and topological corner resonance on the breathing kagome and pyrochlore lattices, Phys. Rev. B **98**, 201402(R) (2018).

[41] M. Ezawa, Non-Hermitian boundary and interface states in nonreciprocal higher-order topological metals and electrical circuits, Phys. Rev. B **99**, 121411(R) (2019).

[42] M. Ezawa, Non-Hermitian higher-order topological states in nonreciprocal and reciprocal systems with their electric-circuit realization, Phys. Rev. B **99**, 201411(R) (2019).

[43] J. Fu, Exact weak bosonic zero modes in a Spin/Fermion chain, Phys. Rev. B **106**, L161412 (2022).

[44] J. Xia, X. Zhang, X. Liu, Y. Zhou, and M. Ezawa, Nonlinear dynamics of the topological helicity wave in a frustrated Skyrmion string, Phys. Rev. B **106**, 054414 (2022).

[45] P. Jordan and E. Wigner, Über das Paulische Äquivalenzverbot, Z. Phys. **47**, 631 (1928).

[46] W. P. Su, J. R. Schrieffer, and A. J. Heeger, Solitons in polyacetylene, Phys. Rev. Lett. **42**, 1698 (1979).

[47] M. Leijnse and K. Flensberg, Quantum information transfer between topological and spin qubit systems, Phys. Rev. Lett. **107**, 210502 (2011).

[48] F. M. D'Angelis, F. A. Pinheiro, D. Guéry-Odelin, S. Longhi, and F. Impens, Fast and robust quantum state transfer in a topological Su-Schrieffer-Heeger chain with next-to-nearest-neighbor interactions, Phys. Rev. Res. **2**, 033475 (2020).

[49] N. E. Palaiodimopoulos, I. Brouzos, F. K. Diakonos, and G. Theocharis, Fast and robust quantum state transfer via a topological chain, Phys. Rev. A **103**, 052409 (2021).

[50] L. Huang, Z. Tan, H. Zhong, and B. Zhu, Fast and robust quantum state transfer assisted by zero-energy interface states in a splicing Su-Schrieffer-Heeger chain, Phys. Rev. A **106**, 022419 (2022).

[51] N. Y. Yao, C. R. Laumann, A. V. Gorshkov, H. Weimer, L. Jiang, J. I. Cirac, P. Zoller, and M. D. Lukin, Topologically protected quantum state transfer in a chiral spin liquid, Nat. Commun. **4**, 1585 (2013).

[52] C. Dlaska, B. Vermersch, and P. Zoller, Robust quantum state transfer via topologically protected edge channels in dipolar arrays, Quantum Sci. Technol. **2**, 015001 (2017).

[53] M. Bello, C. E. Creffield, and G. Platero, Sublattice dynamics and quantum state transfer of doublons in two-dimensional lattices, Phys. Rev. B **95**, 094303 (2017).

[54] Q. Xu, G. Sadiek, and S. Kais, Dynamics of entanglement in a two-dimensional spin system, Phys. Rev. A **83**, 062312 (2011).

[55] G. Sadiek, Q. Xu, and S. Kais, Tuning entanglement and ergodicity in two-dimensional spin systems using impurities, and anisotropy, Phys. Rev. A **85**, 042313 (2012).

[56] Z.-M. Wang and L.-A. Wu, Central symmetry in two-dimensional lattices and quantum information transmission, Phys. Rev. A **87**, 064301 (2013).

[57] G. M. A. Almeida, F. Ciccarello, T. J. G. Apollaro, and A. M. C. Souza, Quantum-state transfer in staggered coupled-cavity arrays, Phys. Rev. A **93**, 032310 (2016).

[58] H. Lang and H. P. Büchler, Topological networks for quantum communication between distant qubits, npj Quantum Inf. **3**, 47 (2017).

[59] S. Hu, Y. Ke, and C. Lee, Topological quantum transport and spatial entanglement distribution via a disordered bulk channel, Phys. Rev. A **101**, 052323 (2020).

[60] J. Zurita, C. E. Creffield, and G. Platero, Fast quantum transfer mediated by topological domain walls, Quantum **7**, 1043 (2023).

[61] W. K. Wootters, Entanglement of formation of an arbitrary state of two qubits, Phys. Rev. Lett. **80**, 2245 (1998).

[62] F. Grusdt, T. Li, I. Bloch, and E. Demler, Tunable spin-orbit coupling for ultracold atoms in two-dimensional optical lattices, Phys. Rev. A **95**, 063617 (2017).

[63] J. Zeiher, J.-Y. Choi, A. Rubio-Abadal, T. Pohl, R. van Bijnen, I. Bloch, and C. Gross, Coherent many-body spin dynamics in a long-range interacting Ising chain, Phys. Rev. X **7**, 041063 (2017).

[64] M. Veldhorst, C. H. Yang, J. C. C. Hwang, W. Huang, J. P. Dehollain, J. T. Muhonen, S. Simmons, A. Laucht, F. E. Hudson, K. M. Itoh, A. Morello, and A. S. Dzurak, A two-qubit logic gate in silicon, Nature (London) **526**, 410 (2015).

[65] Z.-M. Wang, L.-A. Wu, M. Modugno, W. Yao, and B. Shao, Fault-tolerant almost exact state transmission, Sci. Rep. **3**, 3128 (2013).

[66] M. Ezawa, Nonlinearity-induced transition in nonlinear Su-Schrieffer-Heeger model and a nonlinear higher-order topological system, Phys. Rev. B **104**, 235420 (2021).

[67] M. Ezawa, Nonlinear non-Hermitian higher-order topological laser, Phys. Rev. Res. **4**, 013195 (2022).

[68] F. Liu and K. Wakabayashi, Novel topological phase with a zero Berry curvature, Phys. Rev. Lett. **118**, 076803 (2017).

[69] F. Liu, Analytic solution of n-dimensional Su-Schrieffer-Heeger model, arXiv:2304.11933.